nature sustainability

Article

https://doi.org/10.1038/s41893-023-01219-0

# Air quality, health and equity implications of electrifying heavy-duty vehicles

In the format provided by the authors and unedited

## Table of Contents

**This PDF file includes:**

Supplementary Discussion
Supplementary Figures S1 to S13
Supplementary Tables S1 to S7
Supplementary References

## Supplementary Discussion

**WRF-CMAQ Model Set-Up.** The two-way coupled WRF-CMAQ model was used to simulate air pollution concentrations over Southern Lake Michigan at a 1.3 km horizontal resolution following the methodology of [1]. This is done by a) Running a nested WRF-only simulation at (i) 12 km, (ii) 4 km, and (iii) 1.3 km, b) Using the WRF output to create meteorologically informed emissions with SMOKE at 4 km and 1.3 km, c) Running a coupled WRF-CMAQ simulation at 4 km, with boundary conditions from the 12 km WRF simulation and chemical and initial conditions from CAM-Chem [2,3] and d) Running the 1.3 km WRF-CMAQ simulation using meteorology and chemistry boundary conditions from the 4 km run. Both the 4 km and 1.3 km simulations integrate the Carbon Bond Mechanism version 6 and aerosol module version 6 with aqueous chemistry (cb6r3_ae6_aq).

WRF simulations are set with 35 vertical layers with a bottom layer of ~20 m and the following physics schemes: (i) Morrison 2-moment microphysics scheme [4], (ii) Kain-Fritsch (KF2) cumulus cloud parameterization version 2 [5], (iii) Asymmetric Convective Model version 2 (ACM2) [6], and (iv) Pleim-Xiu land surface model [7], The Rapid Radiative Transfer Model for GCMs (RRTMG) [8] was used for both the shortwave and longwave radiation schemes. Further description of the model set-up used to derive baseline pollutant concentrations can be found in Montgomery et al. [9].

**Spatial Surrogates** Spatial surrogates are used to allocate emissions to the grid cell level which together with meteorological data and emission factors results in hourly, speciated, gridded emissions. Spatial surrogates typically consist of highly spatially resolved land use information (e.g., lines representing different road types or polygons representing development intensity) used to allocate emissions at a finer scale. To refine emissions from the county level to our 1.3 km grid cells, we take the fraction of the spatial surrogate within each grid cell with respect to the total amount of the surrogate in the county and multiply that fraction by the county emissions [10].

**Model Evaluation.** In this section we compare the simulated pollutant concentrations for each month and averaged across all four months to observations from the EPA AQS stations within the 1.3km domain (Table S1). The number of available EPA stations within the 1.3km domain varied for each month and pollutant. This comparison is limited given the dearth of EPA observations (125 EPA stations) as compared to the large number of grid cells simulated in our modeling domain (90,720 grid cells) resulting in model-observation comparisons at only 0.14% of all the simulation grid cells. Our simulations generally meet suggested benchmarks [9].

**Vehicle-to-EGU Electricity Assignment and Emission Remapping Algorithm.** In this section we describe in detail the method with which we calculate the increase in electricity demand needed to charge EVs at the county level and allocate this altered electricity demand to electricity generating units (EGUs) based on weighted factors. Our electricity assignment algorithm provides a first order approximation of the behavior of the U.S. electricity grid in response to the electricity demand any substantial EV adoption would incur, however it does not attempt to explicitly simulate dispatch, nor the myriad drivers and regulations that ultimately determine which EGUs serve load.

To estimate the increase in electricity demand, we start by selecting 30% of all HDV VMTs and shifting them to EVMT – electric VMTs. We then calculate the resulting increase in electricity demand per county ($\boldsymbol{tE_c}$) as a function of the $EVMT$ and the charging efficiency ($\boldsymbol{CE}$) per vehicle type ($\boldsymbol{k}$) (Eq. S1). Additionally, we account for the distribution and transmission loss of electricity across the U.S. grid by using a grid gross loss ($\boldsymbol{GGL}$) of 5.1% [11].

$$\boldsymbol{tE_c = \sum_1^k EVMT_{c,k} \cdot CE_k \cdot (1 - GGL)^{-1}} \qquad \text{(S1)}$$

The electricity demand to charge 30% of HDVs ($\boldsymbol{tE_c}$) is then distributed to EGUs by first identifying the portion that would be assigned to renewables (eGRID-2016 dataset; EPA, 2022). Using the NERC region's renewability fraction in which the county lies, we omit that portion of electricity from being assigned to non-renewable EGUs. We also account for the portion of electricity assigned to nuclear EGUs. Secondly, we distribute the remaining electricity demand ($\boldsymbol{E_{c,n}}$) to each non-renewable EGU ($\boldsymbol{j}$) by using an augmented version of an emission remapping algorithm first presented in Schnell et al. [13] (Eq. S2). The augmented algorithm incorporates four main weights:

1. **Location** ($\boldsymbol{n}$) - The county needing the additional electricity and the EGU supplying it must lie within the same NERC (North American Electricity Reliability Corporation) region.
    - Sources: U.S. Census Cartographic boundary shapefiles [14] and NERC shapefiles [15].
2. **Distance** ($\boldsymbol{D_{c,j}}$) - Within the same NERC region, the closest EGU to the county in need of the electricity is preferred to EGUs further away.
    - Sources: Centroid of each county [14] and distance between the each county and surrounding EGUs [12]
3. **Age** ($\boldsymbol{A_j}$**)** The younger the EGU, the larger the fraction of the demand it will supply as opposed to older units. Here we assume age is representative of ramp rate.
    - Sources: Age of each EGU is represented by the average age of all the generators within the EGU or assigned the national EGU age average of 40 years depending on available data [12]
4. **Capacity** ($\boldsymbol{fC_j}$) – EGUs with a higher current net generation capacity are preferred to supply the additional demand.
    - Sources: The eGRID-2016 database [12] is used for Net Generation data and Capacity factors.

$$\boldsymbol{aE_{j,n} = \sum_{c=1}^{c} E_{c,n} \cdot ((1 - fC_j) \cdot tG_j) \cdot \left(A_j - D_{c,j}\right)^{-1}} \qquad \text{(S2)}$$

Finally, we calculate each EGU's emission factor ($\boldsymbol{EF_j}$) which we use to estimate modified emissions by adding the increase in electricity demand ($\boldsymbol{aE_{j,n}}$) to the baseline net annual electricity generation and divide by the facility's net annual generation for 2016. The modified emission rates for each EGU and pollutant ($\boldsymbol{mQ_{s,j}}$) are then calculated by linearly scaling the EGU's baseline pollutant specific emission rate ($\boldsymbol{Q_{s,j}}$) by its emission factor ($\boldsymbol{EF_j}$) (Eq. S3).

$$\boldsymbol{mQ_{s,j} = Q_{s,j} \cdot EF_j} \qquad \text{(S3)}$$

**Seasonality in MDA8$O_3$ differences.** In August, differences in MDA8$O_3$ concentrations between the eHDV scenario and baseline have a similar spatial distribution to annual differences although the spatial extent exhibiting MDA8$O_3$ increases is smaller. This pattern also holds for April, however, MDA8$O_3$ decreases in rural and downwind areas are lesser. Conversely, in October and January we note increases in MDA8$O_3$ concentrations across most of the domain with large increases in metropolitan areas and lesser increases in non-urban regions (Fig. S3). The seasonality of simulated MDA8$O_3$ may be partially explained by the seasonality of VOC-to-$NO_x$ ratios (Table S5). For all months, we simulated baseline VOC/NOx ratios greater than 7 ppbC/ppb in rural regions and less than 5 ppbC/ppb in urban areas except for August. The low VOC/NOx ratios for October, January and April explain the overall increases in MDA8$O_3$ concentration across most of the domain following $NO_X$ emission reductions. In August, simulated baseline rural and urban VOC/NOx ratios are on average 15 ppbC/ppb and 7 ppbC/ppb, respectively. This indicates that the urban environment in August is likely in a transitional regime which explains the small spatial extent of increases in MDA8$O_3$ concentrations in August following eHDV adoption (Fig. S3).

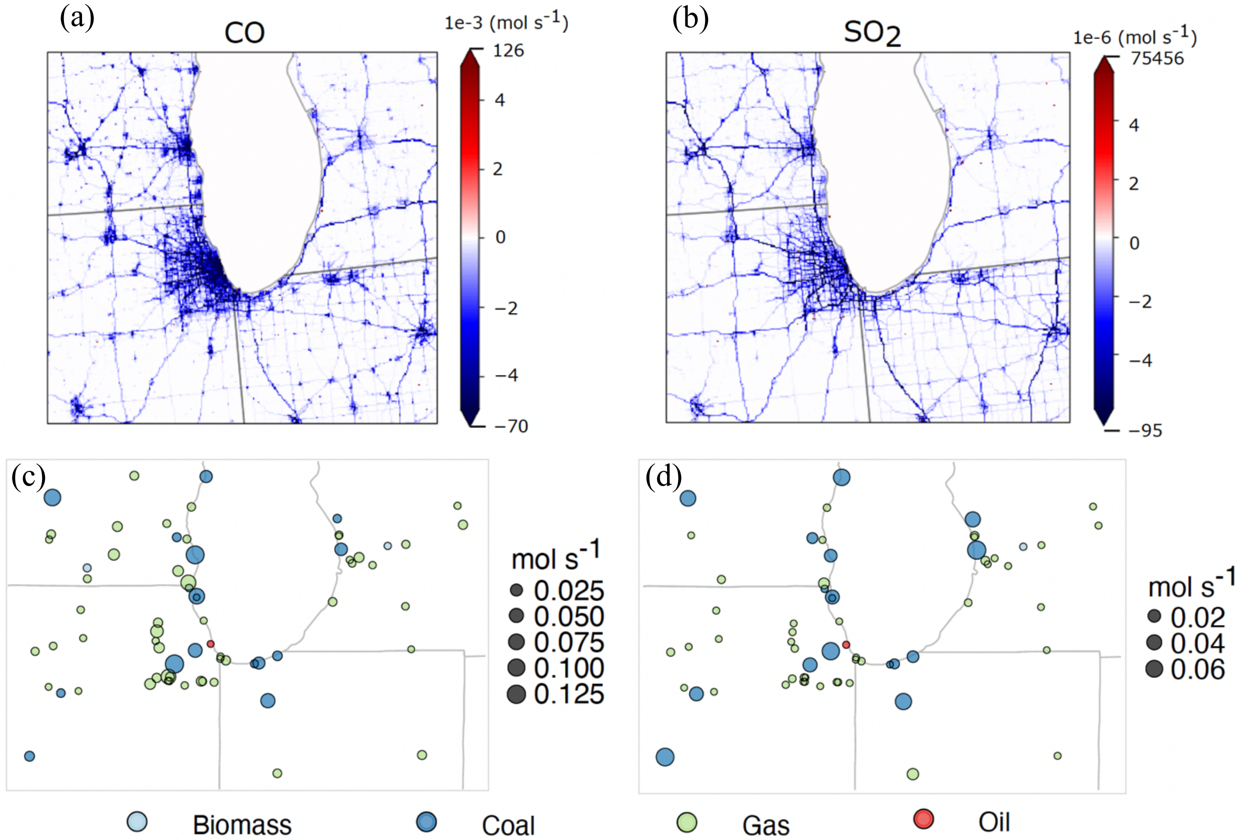


**Fig. S1.** (a) CO and (b) $SO_2$ on-road and EGU emission changes for the 30% adoption of eHDVs as compared to the baseline scenario in mol $s^{-1}$. Numbers at the tails of each scale indicate the minimum and maximum differences in emissions. Point source emission changes for (c) CO and (d) $SO_2$ at EGUs by fuel type (note the magnitude of the maximum values at coal powered EGUs on panels b and d, highlighting the spatial concentration of emissions).

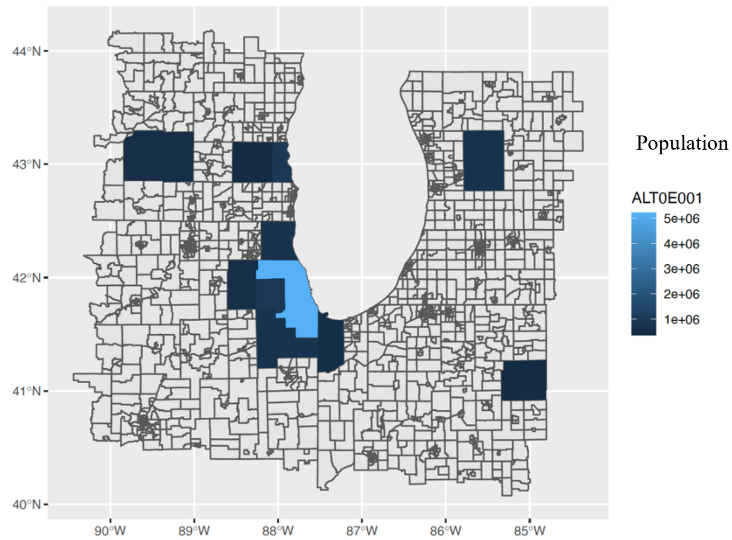


**Fig. S2.** Definition of urban areas derived by selecting the census tracts with the highest (>95$^{th}$ percentile) number of residents within our 1.3 km domain. Areas outside those depicted above represent rural areas.

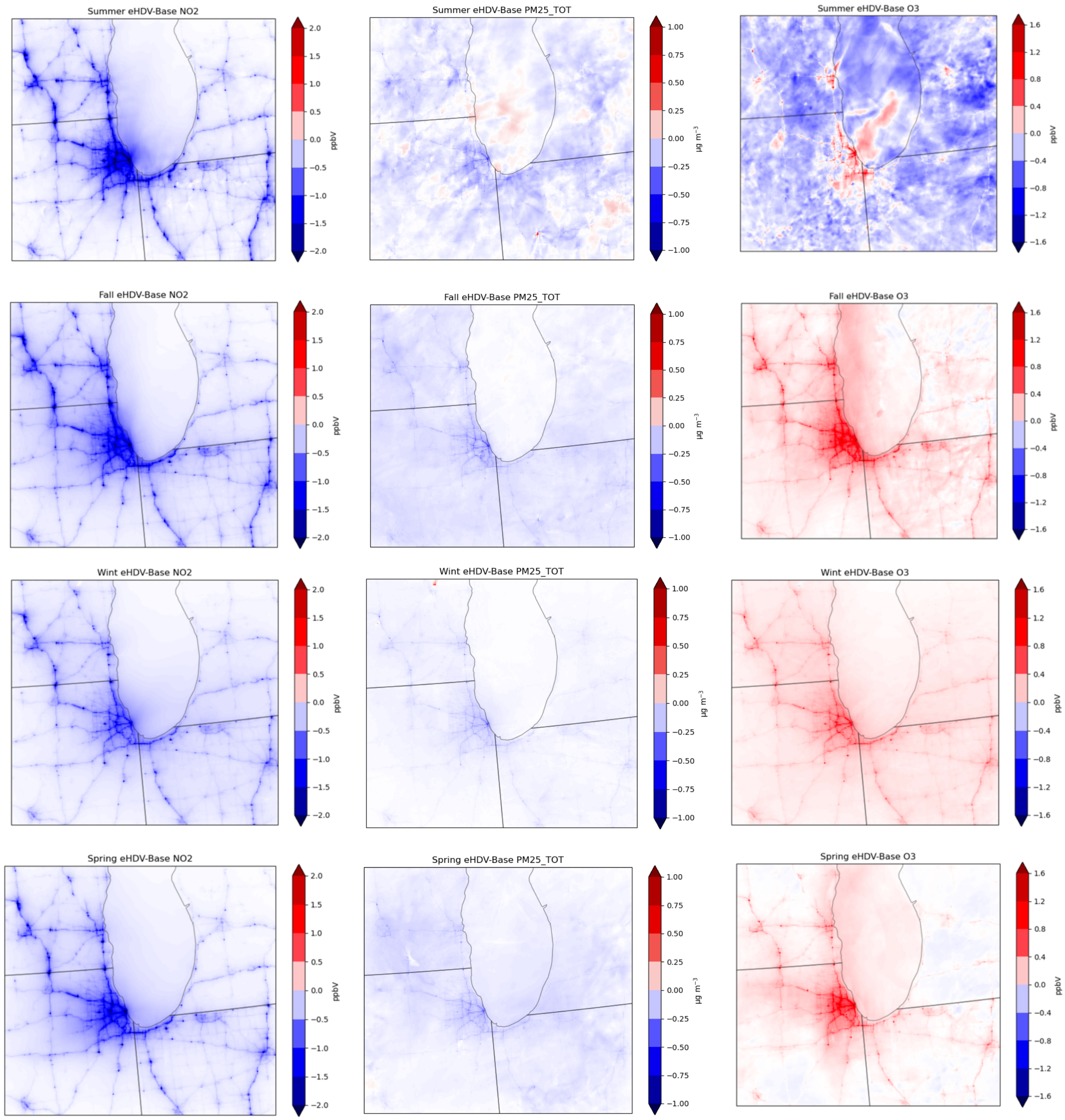


**Fig. S3.** Simulated Baseline $NO_2$ (first column), $PM_{2.5}$ (middle column) and MDA8$O_3$ (third column) concentrations for Aug (top row), Oct (second row), Jan (third row) and Apr (final row).

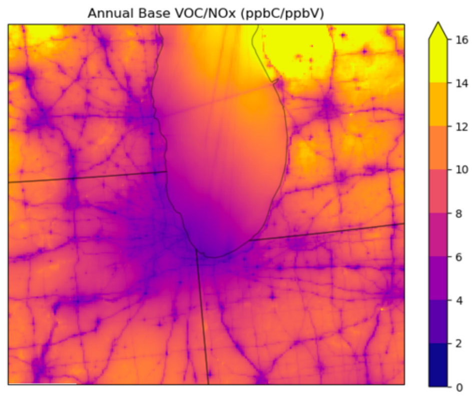


**Fig. S4.** Simulated annual mean baseline VOC to $NO_x$ ratio (ppbC/ppb)

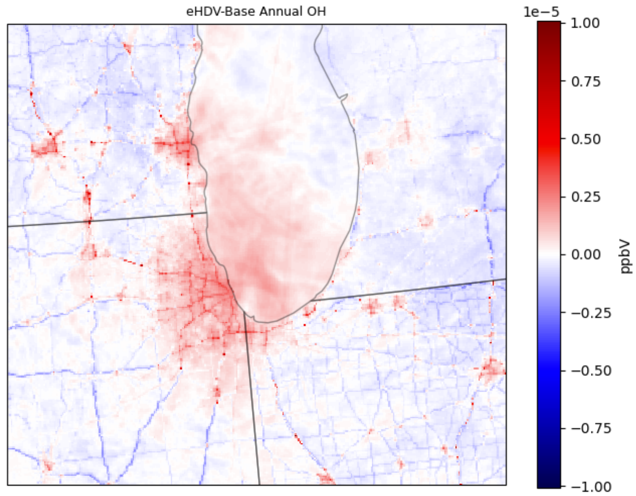


**Fig. S5.** Simulated annual mean differences in OH concentrations (ppb) between the eHDV and baseline simulations.

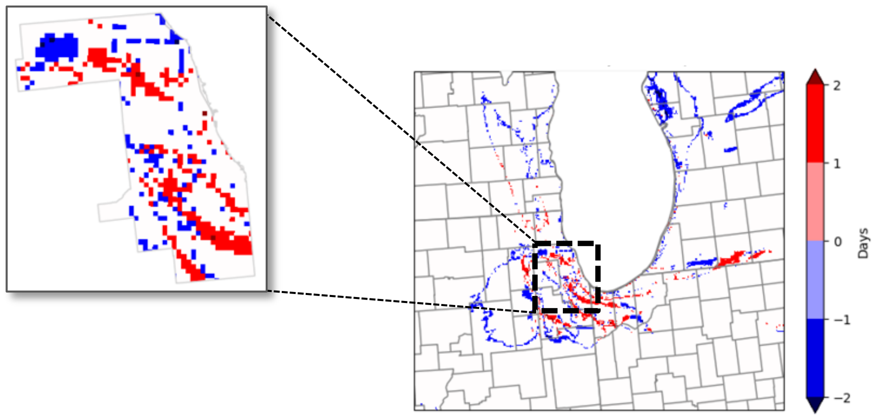


**Fig. S6.** Number of days with simulated differences in MDA8$O_3$ concentrations higher than 70 ppb for the eHDV compared to the baseline scenario across the study domain and Cook County.

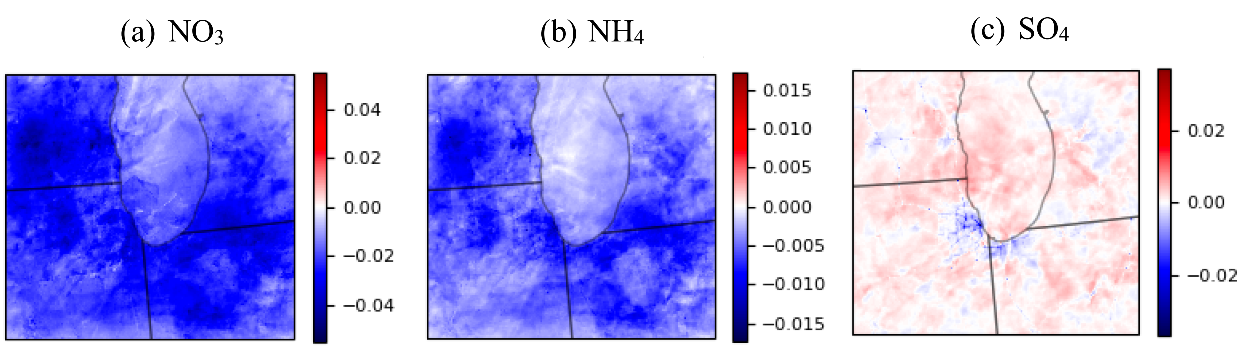


**Fig. S7.** $PM_{2.5}$ composition. Differences in $PM_{2.5}$ composition between the eHDV and baseline simulations for (a) $NO_3$, (b) $NH_4$ and (c) $SO_4$ in $\mu g\ m^{-3}$.

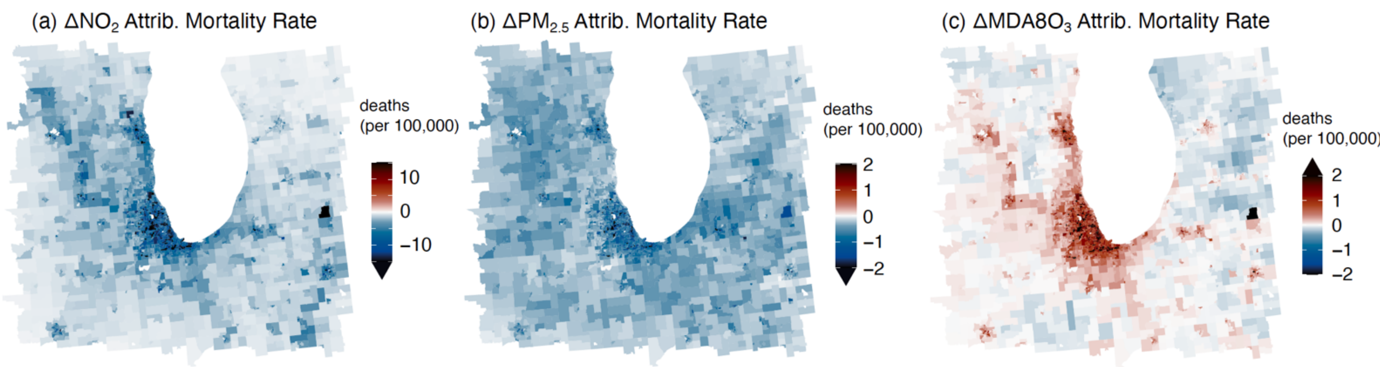


**Fig. S8.** Changes in Attributable Mortality Rates. Spatial distribution of differences in attributable mortality rates associated with long-term exposure to (a) $NO_2$, (b) $PM_{2.5}$ and (c) MDA8$O_3$ concentrations between the eHDV and Baseline estimates at the census tract level (premature deaths per 100,000).

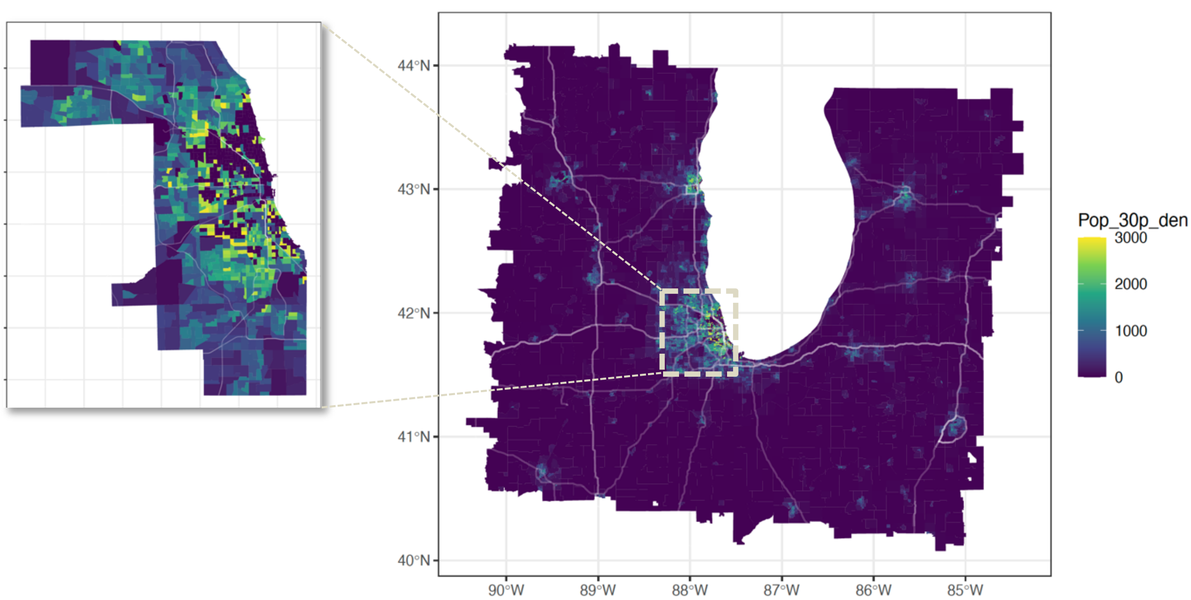


**Fig. S9.** Census Tract-level population density for ages 30 years and over. Population data is from the National Historical Geographic Information System (NHGIS 2015-2019). White lines indicate primary roads.

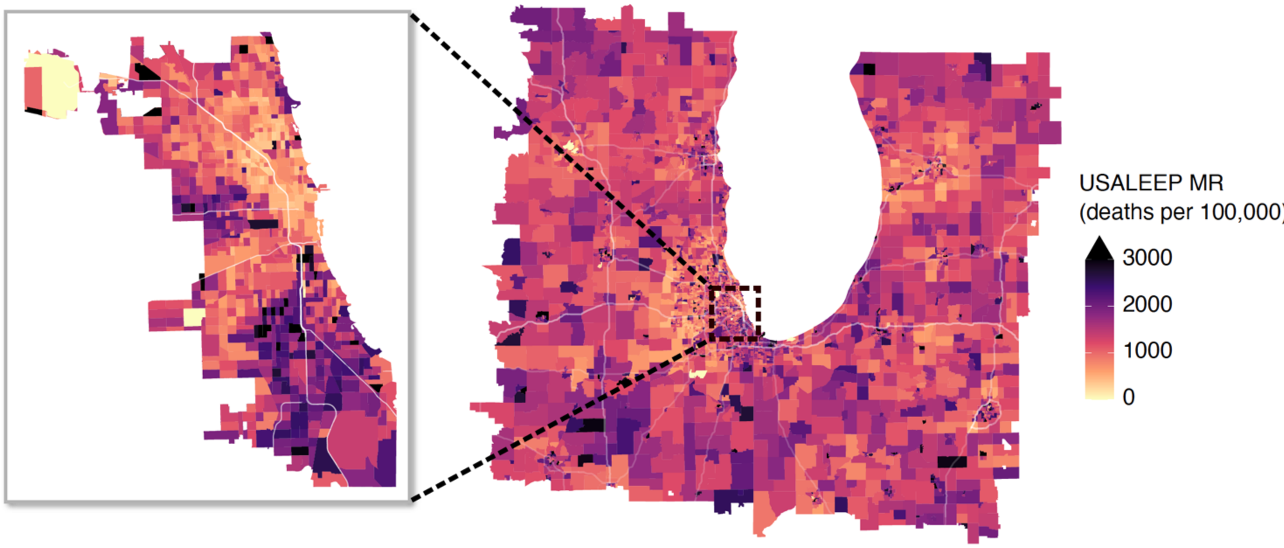


**Fig. S10.** Census Tract-level all-cause baseline mortality data for ages 30 years an over based on baseline mortality rates from Industrial Economic and population data from National Historical Geographic Information System (NHGIS 2015-2019).

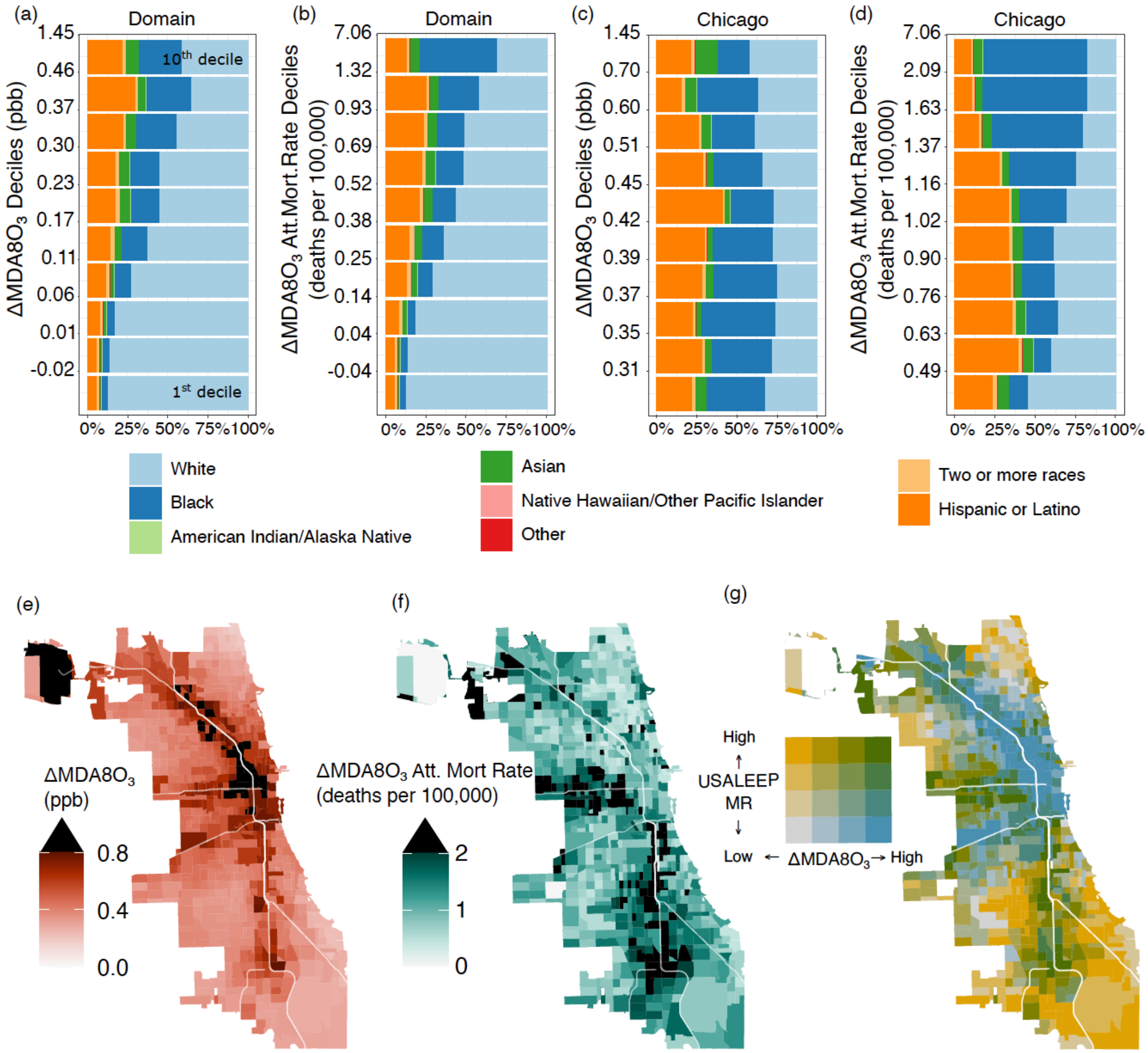


**Fig. S11.** Equity Implications of eHDV adoption. Fractional race and ethnicity of populations for deciles of MDA8O3 concentration changes (a & c) and MDA8O3 attributable mortality rate changes (b & d) for the full model domain (a & b) and the city of Chicago (c & d) with 30% eHDV adoption. (e) Highlight of city of Chicago MDA8O3 concentration changes, (f) MDA8O3 attributable mortality rate changes, and (g) bivariate depiction of the relationship of baseline USALEEP mortality rates with MDA8O3 changes. All race groups except Hispanic or Latino, include only those identifying as non-Hispanic.

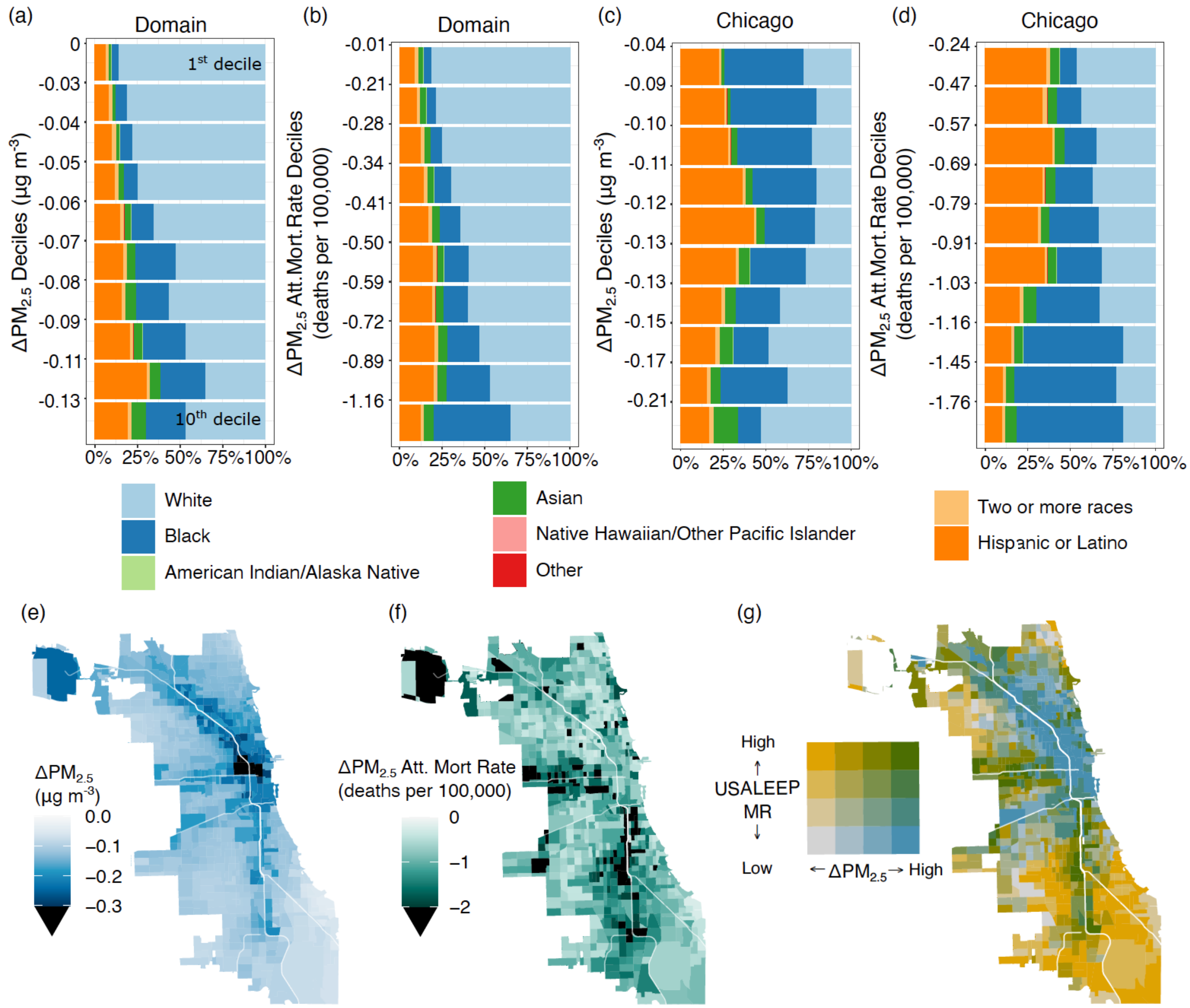


**Fig. S12.** Equity Implications of eHDV adoption. Fractional race and ethnicity of populations for deciles of $PM_{2.5}$ concentration changes (a & c) and $PM_{2.5}$ attributable mortality rate changes (b & d) for the full model domain (a & b) and the city of Chicago (c & d) with 30% eHDV adoption. (e) Highlight of city of Chicago $PM_{2.5}$ concentration changes, (f) $PM_{2.5}$ attributable mortality rate changes, and (g) bivariate depiction of the relationship of baseline USALEEP mortality rates with $PM_{2.5}$ changes. All race groups except Hispanic or Latino, include only those identifying as non-Hispanic.

226

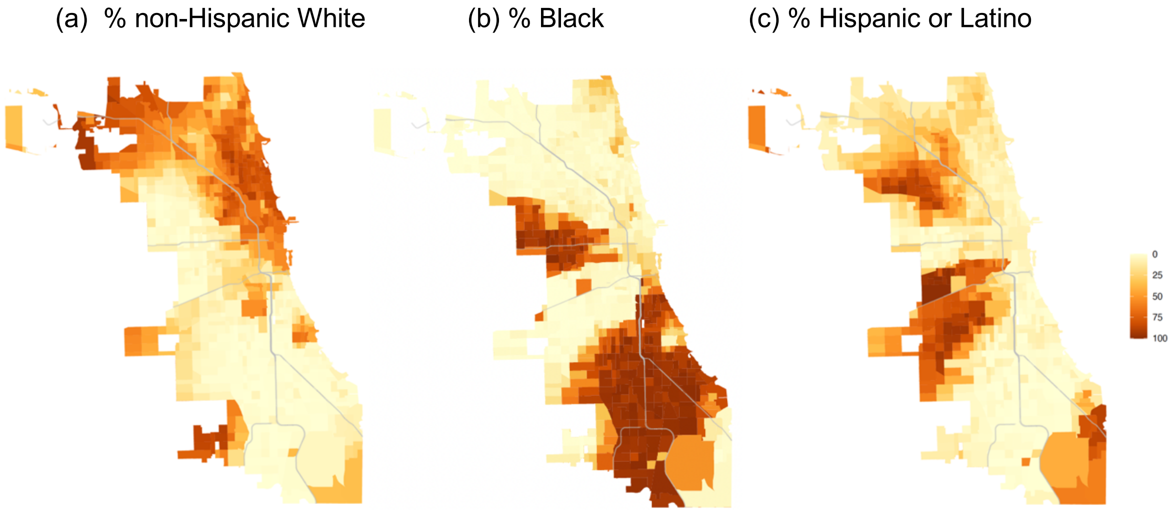


**Fig. S13.** The fraction (in %) of total population within Chicago divided by race and ethnicity; (a) non-Hispanic White, (b) Black and (c) Hispanic or Latino. $NO_2$ changes are negatively correlated with Chicago's Black population ($r$ = -0.20) while $NO_2$ health benefits and baseline mortality rates are positively and more highly correlated with the Black population ($r$ =0.43 and 0.54, respectively).

**Table S1.** WRF-CMAQ performance metrics for simulated $NO_2$, $MDA8O_3$ and $PM_{2.5}$ concentrations at 1.3 km as compared to EPA AQS station observations. $\mu_d$ and $\mu_p$ represent the observed and predicted values, respectively and n represents the number of EPA AQS measurement stations. The number of EPA AQS measurement stations vary for each month with 120, 120, 78 and 125 sites for August and October 2018 and January and April 2019, respectively. Table and values adapted from [9].

| Var | Month | $\mu_d$ | $\mu_p$ | *MB* | *r* |
|---|---|---|---|---|---|
| **$NO_2$** (ppb) (n=15) | Aug 2018 | 10.4 | 10.7 | 0.2 | 0.6 |
| | Oct 2018 | 10.8 | 11.0 | 0.5 | 0.5 |
| | Jan 2019 | 13.1 | 9.6 | -3.5 | 0.6 |
| | Apr 2019 | 11.2 | 10.6 | -0.9 | 0.6 |
| | Annual | 11.4 | 10.5 | -0.9 | 0.6 |
| **$MDA8O_3$** (ppb) (n=67) | Aug 2018 | 42.8 | 53.6 | 10.7 | 0.5 |
| | Oct 2018 | 28.0 | 39.0 | 11.0 | 0.4 |
| | Jan 2019 | 29.7 | 37.3 | 7.5 | 0.6 |
| | Apr 2019 | 44.2 | 55.2 | 11.0 | 0.4 |
| | Annual | 36.2 | 46.3 | 10.1 | 0.5 |
| **$PM_{2.5}$** ($\mu g\ m^{-3}$) (n=25) | Aug 2018 | 12.1 | 7.5 | -4.7 | 0.3 |
| | Oct 2018 | 6.8 | 7.9 | 1.0 | 0.4 |
| | Jan 2019 | 9.4 | 9.8 | 0.3 | 0.5 |
| | Apr 2019 | 7.6 | 6.3 | -1.4 | 0.5 |
| | Annual | 9.0 | 7.9 | -1.2 | 0.4 |

**Table S2.** Baseline Vehicle Miles Traveled (VMT) and Battery Efficiency Rate (BER) for each heavy-duty vehicle type over the entire U.S. The Total Electricity Demand (TED) represents the electricity demand for charging 30% of the U.S. heavy-duty VMT per vehicle type. Each vehicle type listed below is not mapped one-to-one to a regulatory class but instead vehicle types are distributed between regulatory classes based on gross vehicle weight rating (GVWR) classification defined by the Federal Highway Administration (FHWA) [16].

| Vehicle Type | | Heavy Duty Vehicles | | |
|---|---|---|---|---|
| | | VMT (Billion) | BER (kWh/mile) | TED (GWh) |
| Intercity Bus | Class 4 and 5<br>Light HD Gas Vehicles (14,001 -19,500 lbs. GVWR)<br><br>Class 6 and 7<br>Medium HD Gas Vehicles (19,501 -33,000 lbs. GVWR)<br><br>Class 8a and 8b<br>Heavy HD Gas Vehicles (GVWR >33,000 lbs) | 5.04 | 1.61[a] | 2569.94 |
| Transit Bus | Class 4 and 5<br>Light HD Gas Vehicles (14,001 -19,500 lbs. GVWR)<br><br>Class 6 and 7<br>Medium HD Gas Vehicles (19,501 -33,000 lbs. GVWR)<br><br>Class 8a and 8b<br>Heavy HD Gas Vehicles (GVWR >33,000 lbs) | 2.92 | 2.01[b] | 1851.99 |
| School Bus | Class 2b Trucks with 2 Axles and at least 6 Tiers or Class 3<br>Light HD Gas Vehicles (8,501 -14,000 lbs. GVWR)<br><br>Class 4 and 5<br>Light HD Gas Vehicles (14,001 -19,500 lbs. GVWR)<br><br>Class 6 and 7<br>Medium HD Gas Vehicles (19,501 -33,000 lbs. GVWR)<br><br>Class 8a and 8b<br>Heavy HD Gas Vehicles (GVWR >33,000 lbs) | 6.98 | 1.36[c] | 2989.06 |
| Refuse Truck | Class 2b Trucks with 2 Axles and at least 6 Tiers or Class 3<br>Light HD Gas Vehicles (8,501 -14,000 lbs. GVWR)<br><br>Class 4 and 5<br>Light HD Gas Vehicles (14,001 -19,500 lbs. GVWR)<br><br>Class 6 and 7<br>Medium HD Gas Vehicles (19,501 -33,000 lbs. GVWR) | 2.24 | 1.98[d] | 1396.20 |
| Single Unit Short-Haul Truck | Class 2b Trucks with 2 Axles and at least 6 Tiers or Class 3<br>Light HD Gas Vehicles (8,501 -14,000 lbs. GVWR)<br><br>Class 4 and 5<br>Light HD Gas Vehicles (14,001 -19,500 lbs. GVWR) | 62.27 | 2.00[e] | 39372.95 |

| | | | | |
|---|---|---|---|---|
| | Class 6 and 7<br>Medium HD Gas Vehicles (19,501 -33,000 lbs. GVWR) | | | |
| Single Unit Long-Haul Truck | Class 2b Trucks with 2 Axles and at least 6 Tiers or Class 3<br>Light HD Gas Vehicles (8,501 -14,000 lbs. GVWR)<br><br>Class 4 and 5<br>Light HD Gas Vehicles (14,001 -19,500 lbs. GVWR)<br><br>Class 6 and 7<br>Medium HD Gas Vehicles (19,501 -33,000 lbs. GVWR) | 39.42 | 2.00[e] | 24919.99 |
| Motor Home | Class 2b Trucks with 2 Axles and at least 6 Tiers or Class 3<br>Light HD Gas Vehicles (8,501 -14,000 lbs. GVWR)<br><br>Class 4 and 5<br>Light HD Gas Vehicles (14,001 -19,500 lbs. GVWR)<br><br>Class 6 and 7<br>Medium HD Gas Vehicles (19,501 -33,000 lbs. GVWR)<br><br>Class 8a and 8b<br>Heavy HD Gas Vehicles (GVWR >33,000 lbs) | 2.73 | 0.43[f] | 373.68 |
| Combination Short-Haul Truck | Class 6 and 7<br>Medium HD Gas Vehicles (19,501 -33,000 lbs. GVWR)<br><br>Class 8a and 8b<br>Heavy HD Gas Vehicles (GVWR >33,000 lbs) | 56.84 | 2.00[e] | 35937.80 |
| Combination Long-Haul Truck | Class 6 and 7<br>Medium HD Gas Vehicles (19,501 -33,000 lbs. GVWR)<br><br>Class 8a and 8b<br>Heavy HD Gas Vehicles (GVWR >33,000 lbs) | 106.26 | 2.00[e] | 67182.95 |
| Total | | | | 176594.56 |

a[17] b[18] c[19] d[20] e[21] f[22]

**Table S3.** Time averaged percentage differences in on-road and EGU emissions. PEC, $PSO_4$, $PNH_4$ and $PNO_3$ represent the emissions of EC, $SO_4$, $NH_4$ and $NO_3$ aerosols, respectively. VOC emissions only represent anthropogenic emissions and do not include any biogenic VOCs.

| Emissions | Baseline | | Difference (eHDV – Baseline) | | |
|---|---|---|---|---|---|
| | On-road (g/s) | EGUs (g/s) | On-road (g/s) | EGUs (g/s) | Total % Diff |
| CO | 58236.44 | 445.25 | -721.52 | 26.85 | -1.18 |
| $NH_3$ | 2976.38 | 48.93 | -3.73 | 3.61 | 0.00 |
| $NO_x$ | 7281.80 | 657.98 | -575.57 | 41.31 | -6.73 |
| $SO_2$ | 262.22 | 958.40 | -1.80 | 36.69 | +2.86 |
| $CH_4$ | 4365.04 | 39.81 | -15.63 | 3.55 | -0.27 |
| VOC | 11266.01 | 43.13 | -89.25 | 2.58 | -0.77 |
| PEC | 259.50 | 4.77 | -15.93 | 0.33 | -5.90 |
| $PSO_4$ | 40.93 | 9.45 | -1.81 | 0.63 | -2.34 |
| $PNH_4$ | 12.89 | 1.51 | -0.23 | 0.12 | -0.74 |
| $PNO_3$ | 8.46 | 0.72 | -0.12 | 0.06 | -0.64 |

**Table S4.** Average baseline pollutant concentrations for grid cells within which EGUs lie (At EGUs) and all domain grid cells (Domain) for 2 separate experiments (i) using the 2016 grid (wEGU) and (ii) assuming all additional energy is addressed by clean energy (noEGU). Similarly, we include average eHDV pollutions, as well as mean, max and min differences.

| $NO_2$ (ppb) | avgBASE | avgHDV | diffMean | diffMax | diffMin | Region |
|---|---|---|---|---|---|---|
| | 5.67 | 5.34 | -0.33 | -0.02 | -1.27 | At EGUs (wEGU) |
| | 5.67 | 5.32 | -0.35 | -0.03 | -1.30 | At EGUs (noEGU) |
| | 2.81 | 2.65 | -0.16 | -0.01 | -4.91 | Domain (wEGU) |
| | 2.81 | 2.65 | -0.16 | -0.01 | -4.92 | Domain (noEGU) |
| $O_3$ (ppb) | avgBASE | avgHDV | diffMean | diffMax | diffMin | Region |
| | 37.89 | 38.16 | 0.27 | 0.95 | 0.01 | At EGUs (wEGU) |
| | 37.89 | 38.17 | 0.28 | 1.00 | 0.00 | At EGUs (noEGU) |
| | 40.02 | 40.15 | 0.12 | 2.43 | -0.07 | Domain (wEGU) |
| | 40.02 | 40.15 | 0.12 | 2.45 | -0.07 | Domain (noEGU) |
| $PM_{2.5}$ ($\mu g\ m^{-3}$) | avgBASE | avgHDV | diffMean | diffMax | diffMin | Region |
| | 6.73 | 6.68 | -0.05 | -0.01 | -0.17 | At EGUs (wEGU) |
| | 6.73 | 6.67 | -0.06 | -0.02 | -0.19 | At EGUs (noEGU) |
| | 5.52 | 5.48 | -0.04 | 0.05 | -0.50 | Domain (wEGU) |
| | 5.52 | 5.47 | -0.04 | 0.04 | -0.52 | Domain (noEGU) |

**Table S5.** Urban/Rural ratios calculated from annual mean simulated pollutant concentrations at the census tract level using urban and rural definitions as illustrated in Fig.S2.

| **Urban/Rural Ratio** | Baseline | eHDV - Baseline |
|---|---|---|
| $NO_2$ | 2.8 | 3.5 |
| $MDA8O_3$ | 0.9 | 16.5 |
| $PM_{2.5}$ | 1.3 | 2.0 |

**Table S6.** Rural and Urban VOC/$NO_X$ ratios for each simulation month and averaged across all months. Urban and rural definitions are the same as those presented in Fig. S2.

| **VOC/NOx Ratio** | Rural | Urban |
|---|---|---|
| Aug 2018 | 14.57 | 6.89 |
| Oct 2018 | 7.41 | 4.22 |
| Jan 2019 | 7.35 | 4.39 |
| Apr 2019 | 7.93 | 4.34 |
| Annual | 9.04 | 4.88 |

**Table S7. Attributable Mortality Estimates.** Annual mean differences in population-weighted $NO_2$, $PM_{2.5}$ and MDA8$O_3$ concentrations together with the Attributable Fraction (AF) and estimated all-cause mortality associated with long-term exposure to each pollutant. Numbers in brackets indicate the 95% confidence interval associated with the respective coefficient used. Negative numbers indicate avoided deaths while positive numbers indicate additional deaths.

| | Baseline | eHDV - Baseline | | |
|---|---|---|---|---|
| | AF (%) | Annual Mean Poll. Conc. | AF (%) | Attributable Mortality (Deaths) |
| $NO_2$ (ppb) | **6.34** (1.64, 9.30) | **-0.5** | **-0.42** (-0.10, -0.63) | **-590** (-147, -890) |
| $PM_{2.5}$ (μg $m^{-3}$) | **4.61** (1.56, 7.56) | **-0.1** | **-0.05** (-0.02, -0.08) | **-65** (-21, -109) |
| MDA8$O_3$ (ppb) | **8.65** (4.42, 16.54) | **+0.2** | **+0.04** (0.02, 0.08) | **+54** (27, 108) |

## SI References


1. Wong, D. C. *et al.* WRF-CMAQ two-way coupled system with aerosol feedback: Software development and preliminary results. *Geosci Model Dev* **5**, 299–312 (2012).
2. Emmons, L. K. *et al.* The Chemistry Mechanism in the Community Earth System Model Version 2 (CESM2). *J Adv Model Earth Syst* **12**, (2020).
3. Buchholz, R. R., Emmons, L. K., Tilmes, S. & The CESM2 Development Team. CESM2.1/CAM-chem Instantaneous Output for Boundary Conditions. *UCAR/NCAR - Atmospheric Chemistry Observations and Modeling Laboratory.* https://wiki.ucar.edu/display/camchem/CESM2.1%3ACAM-chem+as+Boundary+Conditions (2019) doi:https://doi.org/10.5065/NMP7-EP60.
4. Morrison, H., Thompson, G. & Tatarskii, V. Impact of cloud microphysics on the development of trailing stratiform precipitation in a simulated squall line: Comparison of one- and two-moment schemes. *Mon Weather Rev* **137**, 991–1007 (2009).
5. Kain, J. S. The Kain-Fritsch Convective Parameterization: An Update. *Journal of Applied Meteorology* **43**, 170–181 (2004).
6. Pleim, J. E. A combined local and nonlocal closure model for the atmospheric boundary layer. Part I: Model description and testing. *J Appl Meteorol Climatol* **46**, 1383–1395 (2007).
7. Xiu, A. & Pleim, J. E. Development of a Land Surface Model. Part I: Application in a Mesoscale Meteorological Model. *Journal of Applied Meteorology* **40**, 192–209 (2001).
8. Clough, S. A. *et al.* Atmospheric radiative transfer modeling: A summary of the AER codes. *J Quant Spectrosc Radiat Transf* **91**, 233–244 (2005).
9. Montgomery, A., Schnell, J. L., Adelman, Z., Janssen, M. & Horton, D. E. Simulation of Neighborhood-Scale Air Quality with two-way coupled WRF-CMAQ over Southern Lake Michigan-Chicago Region. *Journal of Geophysical Research: Atmospheres* (2023) doi:10.1029/2022JD037942.
10. CMAS. SMOKE-MOVES and the Emissions Modeling Framework. https://www.cmascenter.org/emf/internal/smoke_moves/ (2015).
11. EPA. *The Emissions & Generation Resource Integrated Database. Technical Guide, eGrid2019.* https://www.epa.gov/sites/default/files/2021-02/documents/egrid2019_technical_guide.pdf (2021).
12. EPA. Emissions & Generation Resource Integrated Database (eGRID). https://www.epa.gov/egrid (2022).
13. Schnell, J. L. *et al.* Air quality impacts from the electrification of light-duty passenger vehicles in the United States. *Atmos Environ* **208**, 95–102 (2019).
14. US Census Bureau. Cartographic Boundary Files. https://www.census.gov/geographies/mapping-files/time-series/geo/cartographic-boundary.html.
15. EIA. NERC Regions. https://atlas.eia.gov/datasets/eia::nerc-regions/about (2020).
16. EPA. *MOVES2014 and MOVES2014a Technical Guidance: Using MOVES to prepare Emission Inventories for State Implementation Plans and Transportation Conformity. EPA-420-B-15-093.* https://nepis.epa.gov/ (2015).
17. EBUSCO. EBUSCO 2.2. https://www.ebusco.com/electric-buses/ebusco-2-2/ (2022).
18. PROTERRA. Revolutionizing Transit. (2022).
19. LION. Electric School Bus. https://thelionelectric.com/en/products/electric (2022).
20. LION ELECTRIC. Make the bright choice. https://pages.thelionelectric.com/all-electric-lion8-refuse-truck-lion-electric/ (2022).
21. TESLA. Semi The Future of Trucking. https://www.tesla.com/semi (2022).
22. IRIDIUM. Iridium Camper Vans. https://www.iridium-wohnmobile.de (2022).